Robotica (2008) volume 26, pp. 345–356. © 2008 Cambridge University Press
doi:10.1017/S0263574707004092 Printed in the United Kingdom

Dynamic model based formation control and obstacle avoidance of multi-robot systems

Celso De La Cruz* and Ricardo Carelli

Instituto de Automática, Universidad Nacional de San Juan, Av. San Martín Oeste 1109, J5400ARL, Argentina.

(Received in Final Form: December 17, 2007. First published online: January 21, 2008)

SUMMARY

This work presents, first, a complete dynamic model of a unicycle-like mobile robot that takes part in a multi-robot formation. A linear parameterization of this model is performed in order to identify the model parameters. Then, the robot model is input-output feedback linearized. On a second stage, for the multi-robot system, a model is obtained by arranging into a single equation all the feedback linearized robot models. This multi-robot model is expressed in terms of formation states by applying a coordinate transformation. The inverse dynamics technique is then applied to design a formation control. The controller can be applied both to positioning and to tracking desired robot formations. The formation control can be centralized or decentralized and scalable to any number of robots. A strategy for rigid formation obstacle avoidance is also proposed. Experimental results validate the control system design.

KEYWORDS: Formation control: Dynamic model: Non-holonomic mobile robots: Nonlinear systems.

1. Introduction

A marked trend in robot applications is calling for controlling coordinately a group of robots assigned to perform a specific task. The motivation for coordinated control lies on the fact that there are tasks which are impossible to perform with just one robot, and other tasks in which working with a number of robots is less expensive than with just one specialized robot. Examples of such tasks are: surveillance operations, search and exploration, rescue, survey and mapping, cooperative handling of objects, and other work. Many of these applications need a formation control to perform the task efficiently.

Formation control strategies can be classified as centralized [13] when there is a monitoring and control of all robots by a central processor; or decentralized [25] when there is no supervisor, every robot has its own controller and the control feedback is only the detected relative positions of each robot respecting their neighbor robots.

Basically, there are three approaches for robot coordination reported in the literature: leader tracking [16], [10], behavior methods [3, 12], and virtual structure techniques. [5, 23] Most of the proposed coordination control systems are not based on dynamic systems and control theory, largely on account of the complexity of multi-robot systems. However, in order to ensure system stability, it is necessy to resort to using the tools from control theory and dynamic systems. For example in [14], the dynamic model of the mobile robot is output feedback linearized and the formation control is designed using passivity techniques, even though the control is based on a sequence of formations and not on a continuous tracking, and the control actions are forces and torques which are not simple to apply to real actuators. In [9], an input-output feedback linearization controller is designed and a switching strategy is used to control formations, although there is a constraint in that the leader velocity is bounded away from zero. In [13], a centralized formation control is proposed to manage omnidirectional robots; the stability of the resulting control system is proved by using Lyapunov theory.

In [1, 6] and [22] the objective is to control the values taken by some *task functions* or *platoon-level functions*, such as the average position of the vehicles in a platoon or the distribution of the vehicles about the average position. In the present work these values are called formation states. In [1] a kinematic control of a platoon of autonomous vehicles was presented. A dynamics-based control of swarms using redundant manipulator technique was developed in [6]. This form of control regulates platoon-level functions while still allowing the individual units have some autonomy degree. In [22] a decentralized control system with minimum inter-vehicle communication was investigated, this control is based on a dynamic model linearized at an equilibrium value.

In this paper, the complete dynamic model of a unicycle-like mobile robot of [26] is modified such that the linear and angular reference velocities are now considered as the input signals. These signals are usual inputs in commercial robots. A linear parameterization of this robot model is also presented. The model is then input-output feedback linearized with a novel internal dynamics analysis. The multi-robot system model is obtained by arranging into a single equation all the feedback linearized robot models. Initially, this multi-robot model is expressed in terms of the robots' absolute positions and their time derivatives. Then, a coordinate transformation is applied to express the multi-robot model in terms of formation states, which can be selected as: the relative positions between robots, the formation position, the formation heading, etc. The technique of inverse dynamics is applied to this multi-robot model

* Corresponding author. E-mail: celsodelacruz@gmail.com

https://doi.org/10.1017/S0263574707004092 Published online by Cambridge University Press

to design the formation control law. The structure of this formation control is centralized and the number of robots should not vary; even though, in some cases, it can be divided into several groups of similar controls, obtaining a formation control scalable to any number of robots. Within these cases, a decentralized formation control can be found. The resulting control law has the distinctive feature that it allows positioning as well as tracking the desired formations. In addition, final actuation on the robots is in terms of linear and angular reference velocities, as usually found in commercial robots. Finally, it is noted that this formation controller is based on the complete nonlinear dynamic model of the robot.

Obstacle avoidance is also developed in this work, based on the concept of impedance with fictitious forces. The novelty in this obstacle avoidance strategy is that a dynamical perimeter enclosing the formation is used to help the formation efficiently avoid the obstacle. The fictitious forces are applied on the perimeter and not on a single robot, thus the formation is maintained while being deviated, and the perimeter changes its shape dynamically in order to let the formation avoid the obstacle successfully.

The paper is organized as follows. In Section 2, the complete dynamic model and its linear parameterization are presented. Section 3 develops the input-output feedback linearization of the robot model. Section 4 presents the formation control and its stability analysis. Section 5 analyzes the scalability of the formation control. Section 6 develops a strategy for rigid formation obstacle avoidance. Section 7 shows experimental results, and finally, in Section 8, some conclusions and suggestions for future work are given.

2. Dynamic Modeling

In this section a unicycle-like mobile robot is considered, which will take part into the multi-robot formation. The unicycle like robot presents the advantages of high mobility, high traction with pneumatic tires, and a simple wheel configuration. [26] Due to these advantages, this robot structure has been utilized in applications such as automating highway maintenance and constructions. The mobile robot is illustrated in Fig. 1, where G is the center of mass; B is the wheel baseline center; $h = [x \quad y]^{\mathrm{T}}$ is the point that is required to track a trajectory; u and $\bar{u}$ are the longitudinal and lateral velocities of the center of mass; ω and ψ are the angular velocity and heading of the robot; d, b, a, e and c are distances; $F_{rrx'}$ and $F_{rry'}$ are the longitudinal and lateral tire forces of the right wheel; $F_{rlx'}$ and $F_{rly'}$ are the longitudinal and lateral tire forces of the left wheel; $F_{cx'}$ and $F_{cy'}$ are the longitudinal and lateral force exerted on C by the castor; $F_{ex'}$ and $F_{ey'}$ are the longitudinal and lateral forces exerted on E by the tool (for example, a robotic arm or a gripper); and τ_e is the moment exerted by the tool.

The force and moment equations for the robot are [7]:

$$\sum F_{x'} = m(\dot{u} - \bar{u}\omega) = F_{rlx'} + F_{rrx'} + F_{ex'} + F_{cx'},$$

$$\sum F_{y'} = m(\dot{\bar{u}} + u\omega) = F_{rly'} + F_{rry'} + F_{ey'} + F_{cy'},$$

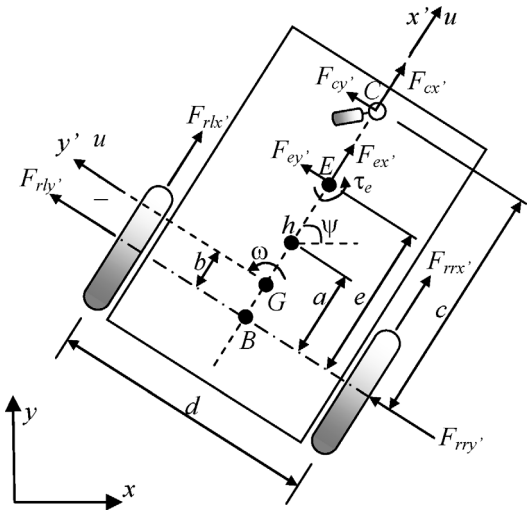


Fig. 1. Parameters of the unicycle-like mobile robot.

$$\sum M_z = I_z\dot{\omega} = \frac{d}{2}(F_{rrx'} - F_{rlx'}) - b(F_{rly'} + F_{rry'}) + (e-b)\,F_{ey'} + (c-b)\,F_{cy'} + \tau_e; \tag{1}$$

where m is the robot mass; and I_z is the robot moment of inertia about the vertical axis located in G. The kinematics of point h is:

$$\begin{aligned} \dot{x} &= u\cos\psi - \bar{u}\sin\psi - (a-b)\,\omega\sin\psi, \\ \dot{y} &= u\sin\psi + \bar{u}\cos\psi + (a-b)\,\omega\cos\psi. \end{aligned} \tag{2}$$

According to [26], velocities u, ω and $\bar{u}$, including the slip speeds, are:

$$\begin{aligned} u &= \frac{1}{2}\left[r\,(\omega_r + \omega_l) + \left(u_r^s + u_l^s\right)\right], \\ \omega &= \frac{1}{d}\left[r\,(\omega_r - \omega_l) + \left(u_r^s - u_l^s\right)\right], \\ \bar{u} &= \frac{b}{d}\left[r\,(\omega_r - \omega_l) + \left(u_r^s - u_l^s\right)\right] + \bar{u}^s, \end{aligned} \tag{3}$$

where r is the right and left wheel radius; ω_r and ω_l are the angular velocities of the right and left wheels; u_r^s and u_l^s are the longitudinal slip speeds of the right and left wheel, and $\bar{u}^s$ is the lateral slip speed of the wheels.

The motor models attained by neglecting the voltage on the inductances are:

$$\tau_r = k_a\,(v_r - k_b\omega_r)\,/R_a, \qquad \tau_l = k_a\,(v_l - k_b\omega_l)\,/R_a. \tag{4}$$

where v_r and v_l are the input voltages applied to the right and left motors; k_b is equal to the voltage constant multiplied by the gear ratio; R_a is the electric resistance constant; τ_r and τ_l are the right and left motor torques multiplied by the gear ratio; and k_a is the torque constant multiplied by the gear ratio. The dynamic equations of the motor-wheels are:

$$\begin{aligned} I_e\dot{\omega}_r + B_e\omega_r &= \tau_r - F_{rrx'}R_t, \\ I_e\dot{\omega}_l + B_e\omega_l &= \tau_l - F_{rlx'}R_t, \end{aligned} \tag{5}$$

https://doi.org/10.1017/S0263574707004092 Published online by Cambridge University Press

where I_e and B_e are the moment of inertia and the viscous friction coefficient of the combined motor rotor, gearbox, and wheel; and R_t is the nominal radius of the tire.

In general, most market-available robots have low level PID velocity controllers to track input reference velocities and do not allow the motor voltage to be driven directly. Therefore, it is useful to express the mobile robot model in a suitable way by considering linear and angular reference velocities as control signals. For this purpose, the velocity controllers are included into the model. In the absence of slips, the point B has only a longitudinal velocity u thus, in general, this velocity will be called linear velocity. To simplify the model, PD velocity controllers have been considered, and are described by the following equation:

$$\begin{bmatrix} v_u \\ v_\omega \end{bmatrix} = \begin{bmatrix} k_{PT}(u_{ref} - u_{me}) - k_{DT}\dot{u}_{me} \\ k_{PR}(\omega_{ref} - \omega_{me}) - k_{DR}\dot{\omega}_{me}, \end{bmatrix}, \tag{6}$$

where:

$$u_{me} = \frac{1}{2}[r(\omega_r + \omega_l)], \quad \omega_{me} = \frac{1}{d}[r(\omega_r - \omega_l)].$$
$$v_u = \frac{v_l + v_r}{2}, \quad v_\omega = \frac{v_r - v_l}{2}.$$

Variables $\dot{u}_{ref}$ and $\dot{\omega}_{ref}$ are neglected in (6) to further simplify the model.

From (1), (2), (3), (4), (5), and (6) the following dynamic model of the mobile robot is obtained (see Appendix for details):

$$\begin{bmatrix} \dot{x} \\ \dot{y} \\ \dot{\psi} \\ \dot{u} \\ \dot{\omega} \end{bmatrix} = \begin{bmatrix} u\cos\psi - a\omega\sin\psi \\ u\sin\psi + a\omega\cos\psi \\ \omega \\ \frac{\bar{\theta}_3^0}{\bar{\theta}_1^0}\omega^2 - \frac{\bar{\theta}_4^0}{\bar{\theta}_1^0}u \\ -\frac{\bar{\theta}_5^0}{\bar{\theta}_2^0}u\omega - \frac{\bar{\theta}_6^0}{\bar{\theta}_2^0}\omega \end{bmatrix} + \begin{bmatrix} 0 & 0 \\ 0 & 0 \\ 0 & 0 \\ \frac{1}{\bar{\theta}_1^0} & 0 \\ 0 & \frac{1}{\bar{\theta}_2^0} \end{bmatrix} \begin{bmatrix} u_{ref} \\ \omega_{ref} \end{bmatrix} + \begin{bmatrix} \delta_x \\ \delta_y \\ 0 \\ \bar{\delta}_u \\ \bar{\delta}_\omega \end{bmatrix}. \tag{7}$$

The parameters of the dynamic model are:

$$\bar{\theta}_1^0 = \left(\frac{R_a}{k_a}(mR_t r + 2I_e) + 2rk_{DT}\right) \Big/ (2rk_{PT}),$$
$$\bar{\theta}_2^0 = \left(\frac{R_a}{k_a}(I_e d^2 + 2R_t r(I_z + mb^2)) + 2rdk_{DR}\right) \Big/ (2rdk_{PR}), \tag{8}$$
$$\bar{\theta}_3^0 = \frac{R_a}{k_a} mbR_t/(2k_{PT}), \; \bar{\theta}_4^0 = \frac{R_a}{k_a}\left(\frac{k_a k_b}{R_a} + B_e\right) \Big/ (rk_{PT}) + 1,$$
$$\bar{\theta}_5^0 = \frac{R_a}{k_a} mbR_t/(dk_{PR}),$$
$$\bar{\theta}_6^0 = \frac{R_a}{k_a}\left(\frac{k_a k_b}{R_a} + B_e\right) d/(2rk_{PR}) + 1. \tag{9}$$

The elements of the uncertainty vector $[\delta_x \; \delta_y \; 0 \; \bar{\delta}_u \; \bar{\delta}_\omega]^T$ are:

$$\delta_x = -\bar{u}^s \sin\psi,$$
$$\delta_y = \bar{u}^s \cos\psi,$$

$$\bar{\delta}_u = \frac{R_t R_a}{2\bar{\theta}_1^0 k_{PT} k_a}\left(m\omega\bar{u}^s + F_{ex'} + F_{cx'}\right) + \frac{\bar{\theta}_4^0}{2\bar{\theta}_1^0}\left(u_r^s + u_l^s\right) + \left(\frac{I_e R_a + rk_a k_{DT}}{2\bar{\theta}_1^0 rk_{PT}k_a}\right)\left(\dot{u}_r^s + \dot{u}_l^s\right),$$
$$\bar{\delta}_\omega = \frac{\bar{\theta}_6^0}{\bar{\theta}_2^0 d}\left(u_r^s - u_l^s\right) + \left(\frac{I_e R_a d + 2rk_a k_{DR}}{2\bar{\theta}_2^0 rk_{PR}k_a d}\right)\left(\dot{u}_r^s - \dot{u}_l^s\right) - \frac{\bar{\theta}_5^0}{\bar{\theta}_2^0}\dot{\bar{u}}^s + \frac{R_t R_a}{\bar{\theta}_2^0 dk_{PR}k_a}(eF_{ey'} + cF_{cy'} + \tau_e).$$

Accelerations $\dot{u}$ and $\dot{\omega}$ do not depend on the states ψ, x and y; then, the dynamics of u and ω can be expressed as follows:

$$\begin{bmatrix} \dot{u} \\ \dot{\omega} \end{bmatrix} = \begin{bmatrix} \frac{\bar{\theta}_3^0}{\bar{\theta}_1^0}\omega^2 - \frac{\bar{\theta}_4^0}{\bar{\theta}_1^0}u + \frac{1}{\bar{\theta}_1^0}u_{ref} \\ -\frac{\bar{\theta}_5^0}{\bar{\theta}_2^0}u\omega - \frac{\bar{\theta}_6^0}{\bar{\theta}_2^0}\omega + \frac{1}{\bar{\theta}_2^0}\omega_{ref} \end{bmatrix} + \begin{bmatrix} \bar{\delta}_u \\ \bar{\delta}_\omega \end{bmatrix}.$$

By re-arranging—and disregarding the uncertainty vector to consider a nominal model—the linear parameterization is attained:

$$\begin{bmatrix} \dot{u} & 0 & -\omega^2 & u & 0 & 0 \\ 0 & \dot{\omega} & 0 & 0 & u\omega & \omega \end{bmatrix} \bar{\theta}^0 = \begin{bmatrix} u_{ref} \\ \omega_{ref} \end{bmatrix}, \tag{10}$$

where $\bar{\theta}^0 = [\bar{\theta}_1^0 \;\; \bar{\theta}_2^0 \;\; \bar{\theta}_3^0 \;\; \bar{\theta}_4^0 \;\; \bar{\theta}_5^0 \;\; \bar{\theta}_6^0]^T$.

Then, the parameters $\bar{\theta}^0$ of the nominal model can be easily identified by using an appropriate identification method.

3. Input-Output Feedback Linearization of the Model

In order to perform the input-output feedback linearization [21] of model (7), the output vector is defined as:

$$h = \begin{bmatrix} x \\ y \end{bmatrix}. \tag{11}$$

https://doi.org/10.1017/S0263574707004092 Published online by Cambridge University Press

Considering model (7), the first and second time derivatives of (11) can be expressed as:

$$\dot{h} = \begin{bmatrix} \dot{x} \\ \dot{y} \end{bmatrix} = \begin{bmatrix} u\cos\psi - a\omega\sin\psi \\ u\sin\psi + a\omega\cos\psi \end{bmatrix} + \begin{bmatrix} \delta_x \\ \delta_y \end{bmatrix}, \tag{12}$$

$$\ddot{h} = \begin{bmatrix} -u\omega\sin\psi - a\omega^2\cos\psi \\ u\omega\cos\psi - a\omega^2\sin\psi \end{bmatrix} + \begin{bmatrix} \cos\psi & -a\sin\psi \\ \sin\psi & a\cos\psi \end{bmatrix} \times \left(\begin{bmatrix} \frac{\bar{\theta}_3^0}{\bar{\theta}_1^0}\omega^2 - \frac{\bar{\theta}_4^0}{\bar{\theta}_1^0}u \\ -\frac{\bar{\theta}_5^0}{\bar{\theta}_2^0}u\omega - \frac{\bar{\theta}_6^0}{\bar{\theta}_2^0}\omega \end{bmatrix} + \begin{bmatrix} \frac{1}{\bar{\theta}_1^0} & 0 \\ 0 & \frac{1}{\bar{\theta}_2^0} \end{bmatrix} \begin{bmatrix} u_{ref} \\ \omega_{ref} \end{bmatrix} \right) + \eta, \tag{13}$$

where:

$$\eta = \begin{bmatrix} \cos\psi & -a\sin\psi \\ \sin\psi & a\cos\psi \end{bmatrix} \begin{bmatrix} \bar{\delta}_u \\ \bar{\delta}_\omega \end{bmatrix} + \begin{bmatrix} \dot{\delta}_x \\ \dot{\delta}_y \end{bmatrix}.$$

From (12) and (13), it can be noted that the system has a total relative degree equal to 4. Considering (13) the following control input is obtained:

$$\begin{bmatrix} u_{ref} \\ \omega_{ref} \end{bmatrix} = \begin{bmatrix} \bar{\theta}_1^0 & 0 \\ 0 & \bar{\theta}_2^0 \end{bmatrix} \left(\begin{bmatrix} \cos\psi & \sin\psi \\ -\frac{1}{a}\sin\psi & \frac{1}{a}\cos\psi \end{bmatrix} \times \left(\upsilon - \begin{bmatrix} -u\omega\sin\psi - a\omega^2\cos\psi \\ u\omega\cos\psi - a\omega^2\sin\psi \end{bmatrix} \right) - \begin{bmatrix} \frac{\bar{\theta}_3^0}{\bar{\theta}_1^0}\omega^2 - \frac{\bar{\theta}_4^0}{\bar{\theta}_1^0}u \\ -\frac{\bar{\theta}_5^0}{\bar{\theta}_2^0}u\omega - \frac{\bar{\theta}_6^0}{\bar{\theta}_2^0}\omega \end{bmatrix} \right), \tag{14}$$

where υ is the new input, which is defined in the formation control design. Equation (14) is constrained to a nonzero value of a. Substituting (14) into (13), the input-output feedback linearized system can be expressed as

$$\ddot{h} = \upsilon + \eta. \tag{15}$$

The following inequality is obtained from (12):

$$|\omega| \leq |1/a| C_{h\delta}, \quad \text{where } C_{h\delta} = \max(\|\dot{h}\|) + \max(|\bar{u}^s|).$$

Let $\omega_{\max}$ be the saturation value of $|\omega|$. Then, to avoid the saturation of ω, the following condition must be met:

$$|a| \geq C_{h\delta}/\omega_{\max}. \tag{16}$$

The saturation of ω is considered because, in general, commercial mobile robots specify limits to their velocities.

In order to find the internal dynamics, the following map is considered: [14]

$$\gamma = \Gamma(X) = \begin{bmatrix} x \\ y \\ u\cos\psi - a\omega\sin\psi \\ u\sin\psi + a\omega\cos\psi \\ \psi \end{bmatrix}, \tag{17}$$

where $X = [x \;\; y \;\; \psi \;\; u \;\; \omega]^T$. This map defines a diffeomorphism whose inverse is:

$$X = \Gamma^{-1}(\gamma) = \begin{bmatrix} \gamma_1 \\ \gamma_2 \\ \gamma_5 \\ \gamma_3\cos\gamma_5 + \gamma_4\sin\gamma_5 \\ -\frac{1}{a}\gamma_3\sin\gamma_5 + \frac{1}{a}\gamma_4\cos\gamma_5 \end{bmatrix}. \tag{18}$$

where γ_i is the i-th element of vector γ.

The input-output feedback linearized model expressed in the new coordinates is:

$$\dot{\gamma} = \begin{bmatrix} \gamma_3 + \delta_x \\ \gamma_4 + \delta_y \\ \upsilon_1 + \eta_1 - \dot{\delta}_x \\ \upsilon_2 + \eta_2 - \dot{\delta}_y \\ -\frac{1}{a}\gamma_3\sin\gamma_5 + \frac{1}{a}\gamma_4\cos\gamma_5 \end{bmatrix}. \tag{19}$$

where υ_i is the i-th element of vector υ; and η_i is the i-th element of vector η. From (19) the internal dynamics is obtained:

$$\dot{\gamma}_5 = -\frac{1}{a}\gamma_3\sin\gamma_5 + \frac{1}{a}\gamma_4\cos\gamma_5, \tag{20}$$

which is unobservable and uncontrollable. From (17), $\gamma_5 = \psi$ is attained. Analyzing ψ in (7) and (14), it can be concluded that it is not necessary to bound this angle. However, $\dot{\gamma}_5 = \dot{\psi} = \omega$ needs to be bounded. The following analysis proves the boundedness of $\dot{\gamma}_5$:

$$|\dot{\gamma}_5| = \left| -\frac{1}{a}\gamma_3\sin\gamma_5 + \frac{1}{a}\gamma_4\cos\gamma_5 \right| \leq \left| \frac{1}{a} \right| (|\gamma_3| + |\gamma_4|). \tag{21}$$

In Section 4, the formation control guarantees that $\dot{x} \to \dot{x}_d$ or at least $\dot{x}$ gets into a neighborhood of $\dot{x}_d$, independently of the internal dynamics; then:

$$|\dot{x} - \dot{x}_d| \leq C_{xpe}, \tag{22}$$

where C_{xpe} is a bound for $|\dot{x} - \dot{x}_d|$. From (12) and (17), $\gamma_3 = \dot{x} - \delta_x$ is obtained. Then, a bound for $|\gamma_3|$ is calculated as follows:

$$\begin{gathered} |\gamma_3| = |\dot{x} - \delta_x - \dot{x}_d + \dot{x}_d| \leq |\dot{x} - \dot{x}_d| + |\dot{x}_d| + |\delta_x|, \\ |\gamma_3| \leq C_{xpe} + C_{xpd} + C_{\delta x} = C_{\gamma 3}, \end{gathered} \tag{23}$$

https://doi.org/10.1017/S0263574707004092 Published online by Cambridge University Press

where C_{xpd} is a bound for $|\dot{x}_d|$; and $C_{\delta x}$ is a bound for $|\delta_x|$. Similarly, a bound for $|\gamma_4|$ can be calculated

$$|\gamma_4| \leq C_{ype} + C_{ypd} + C_{\delta y} = C_{\gamma 4}, \tag{24}$$

where C_{ype} is a bound for $|\dot{y} - \dot{y}_d|$; C_{ypd} is a bound for $|\dot{y}_d|$; and $C_{\delta y}$ is a bound for $|\delta_y|$. Using (23) and (24) in (21):

$$|\dot{\gamma}_5| \leq \left|\frac{1}{a}\right| (|\gamma_3| + |\gamma_4|) \leq \left|\frac{1}{a}\right| (C_{\gamma 3} + C_{\gamma 4}). \tag{25}$$

Then, it can be concluded that $\dot{\gamma}_5 = \dot{\psi} = \omega$ is bounded and the internal dynamics (20) shows a good behavior.

4. Formation Control

In the formation control analysis, it is assumed that the model parameters are time-invariant. The input-output feedback linearized model of the i-th mobile robot in a multi-robot system is defined as:

$$\ddot{h}^i = \upsilon^i + \eta^i.$$

Then, the model of the multi-robot system with n mobile robots is:

$$\ddot{\xi} = \mu + \Pi, \tag{26}$$

where $\xi = [(h^1)^T \ldots (h^n)^T]^T$, $\mu = [(\upsilon^1)^T \ldots (\upsilon^n)^T]^T$, and $\Pi = [(\eta^1)^T \ldots (\eta^n)^T]^T$. The elements of ξ and $\dot{\xi}$ are considered the system trivial states.

A variable z^1 is defined as the vector that contains the formation variables: relative positions between robots, centroid position, formation heading, etc. A variable z^2 is defined as the time derivative of z^1, thus $z^2 = \dot{z}^1$. A coordinate transformation is performed in order to express the multi-robot system model (26) in terms of the formation state vector $z = [(z^1)^T (z^2)^T]^T$. To this aim it is defined a smooth mapping ϕ_1 from ξ to z^1, with a smooth inverse ϕ_1^{-1}. Now, it is obtained a mapping ϕ from the state vector $[\xi^T \dot{\xi}^T]^T$ to the formation state vector z:

$$\begin{bmatrix} z^1 \\ z^2 \end{bmatrix} = \begin{bmatrix} \phi_1(\xi) \\ J(\xi)\dot{\xi} \end{bmatrix} = \phi(\xi, \dot{\xi}), \quad \text{where } J(\xi) = \frac{\partial \phi_1(\xi)}{\partial \xi}. \tag{27}$$

This map defines a diffeomorphism which inverse is:

$$\begin{bmatrix} \xi \\ \dot{\xi} \end{bmatrix} = \begin{bmatrix} \phi_1^{-1}(z^1) \\ \bar{J}(z^1)z^2 \end{bmatrix} = \phi^{-1}(z), \quad \text{where } \bar{J}(z^1) = \frac{\partial \phi_1^{-1}(z^1)}{\partial z^1}. \tag{28}$$

From (28), the time derivative of $\dot{\xi}$ is:

$$\ddot{\xi} = \frac{d(\bar{J}(z^1)z^2)}{dt} = \dot{\bar{J}}(z)z^2 + \bar{J}(z^1)\dot{z}^2. \tag{29}$$

By substituting (26) into (29) the new representation of the multi-robot system in terms of the formation state vector z is obtained:

$$\dot{z}^2 = -\bar{J}(z^1)^{-1}\dot{\bar{J}}(z)z^2 + \bar{J}(z^1)^{-1}\mu + \bar{J}(z^1)^{-1}\Pi. \tag{30}$$

The multi-robot system model (30) is expressed in terms of formation states z^1 and z^2. Now, the formation control can be designed and its stability can be analyzed in the formation state space. The analysis is made on the formation state space because we want the multi-robot system to reach a desired formation state.

The following inverse dynamics formation control law is proposed:

$$\mu = \bar{J}(z^1)(K_1\tilde{z}^1 + K_2\tilde{z}^2 + \dot{z}_d^2) + \dot{\bar{J}}(z)z^2, \tag{31}$$

where $\tilde{z}^1 = z_d^1 - z^1$; $\tilde{z}^2 = z_d^2 - z^2$; $z_d^2 = \dot{z}_d^1$; $z_d = [(z_d^1)^T (z_d^2)^T]^T$ is the desired formation state vector; $K_1 > 0$ and $K_2 > 0$ are positive definite matrixes. Then, the closed loop system obtained by substituting the controller of (31) into the system model of (30) is:

$$-\bar{J}(z^1)^{-1}\Pi = K_1\tilde{z}^1 + K_2\tilde{z}^2 + \dot{\tilde{z}}^2, \tag{32}$$

which can be expressed as:

$$\dot{\tilde{z}} = \mathrm{A}_z\tilde{z} - [0 \quad \bar{\Pi}^T]^T, \tag{33}$$

where $\bar{\Pi} = \bar{J}(z^1)^{-1}\Pi$; $\tilde{z} = [(\tilde{z}^1)^T \quad (\tilde{z}^2)^T]^T = z_d - z$; and:

$$\mathrm{A}_z = \begin{bmatrix} 0 & I_{2n\times 2n} \\ -K_1 & -K_2 \end{bmatrix}. \tag{34}$$

In (34), $I_{2n\times 2n}$ represents the $2n \times 2n$ identity matrix. Let K_1 and K_2 be diagonal matrices with positive elements different from zero. From these considerations, A_z is Hurwitz.

The following Lyapunov candidate and its time derivative are now considered:

$$\begin{aligned} V(\tilde{z}) &= \tilde{z}^T P\tilde{z} > 0; \quad P = P^T > 0, \\ \dot{V}(\tilde{z}) &= -\tilde{z}^T Q\tilde{z} - 2\tilde{z}^T P[0 \quad \bar{\Pi}^T]^T, \end{aligned} \tag{35}$$

where:

$$Q = -\mathrm{A}_z^T P - P\mathrm{A}_z. \tag{36}$$

Matrix Q is chosen as $Q = I_{4n\times 4n}$, where $I_{4n\times 4n}$ is the $4n \times 4n$ identity matrix. Matrix P is calculated from (36). Since A_z is Hurwitz, it is verified that $P = P^T > 0$. A sufficient condition for the second of (35) to be negative definite is:

$$\|\tilde{z}\| > 2\|P[0 \quad \bar{\Pi}^T]^T\|. \tag{37}$$

Let us consider the vector $\bar{\Pi}$ to be bounded. Then, there is a bounded neighborhood of the origin, where the formation error vector $\tilde{z}$ will be confined after a finite time. In absence of uncertainties, $\bar{\Pi} = 0$ and $z \to z_d$ with $t \to \infty$.

Remark 1. The proposed controller is able to track a moving or continuously varying desired formation.

https://doi.org/10.1017/S0263574707004092 Published online by Cambridge University Press

Remark 2. The controller needs either the sensorial information from the direct measurement of formation state vector z or the calculation of these states by measuring the trivial state vector $[\xi^T \ \dot{\xi}^T]^T$. In the last case, equation (27) has to be used to be replaced into the control law (31). If necessary, the following equations—obtained from (27) and (28)—can be used as well:

$$\bar{J}(z^1) = J(\xi)^{-1}, \quad \dot{\bar{J}}(z)z^2 = -J(\xi)^{-1}\dot{J}(\xi,\dot{\xi})\dot{\xi}. \tag{38}$$

Remark 3. $\phi^{-1}(z) \to \phi^{-1}(z_d)$ with $z \to z_d$ because $\phi^{-1}(.)$ is a continuous function. Therefore, from (28) $\xi \to \xi_d$ and $\dot{\xi} \to \dot{\xi}_d$ with $z \to z_d$, where $[\xi_d^T \ \dot{\xi}_d{}^T]^T = \phi^{-1}(z_d)$.

5. Scalability of the Formation Control

One of the important aspects of a formation strategy is scalability. Scalability means that the approach could easily be scaled to any number of agents [4], i.e. we can add robots to the formation with just few changes to the formation control.

This section presents two proposals for mapping ϕ_1, defined in (27) of the previous section. As it will be shown, these mappings allow a scalable formation control to any number of robots. Unlike the second mapping, the first mapping also generates a decentralized formation control law, in the sense that neither inter-robot communication nor central processing is needed if each robot has an appropriate sensor mounted on it.

First mapping ϕ_1

The vector ξ is defined as follows:

$$\xi = \begin{bmatrix} h^1 \\ h^2 \\ \vdots \\ h^n \end{bmatrix} = [x^1 \quad y^1 \quad x^2 \quad y^2 \quad \cdots \quad x^n \quad y^n]^{\mathrm{T}}. \tag{39}$$

Let us consider the leader-follower formation scheme of Fig. 2. This scheme is similar to that of, [15 with the difference in that, in Fig. 2, the angles α_i are measured relative to the x-axis, whereas in [15 they are measured with respect to the direction of robot 1.

Choosing the formation variables as in Fig. 2, the following mapping ϕ_1 is obtained:

$$z^1 = \phi_1(\xi) = [x^1 \quad y^1 \quad l_2 \quad \alpha_2 \quad l_3 \quad \alpha_3 \quad \cdots \quad l_n \quad \alpha_n]^{\mathrm{T}}, \tag{40}$$

where:

$$\begin{aligned} l_i &= \sqrt{(x^i - x^1)^2 + (y^i - y^1)^2}; \quad i = 2, 3, \ldots, n, \\ \alpha_i &= f_{\zeta i}(x^i - x^1, y^i - y^1); \quad i = 2, 3, \ldots, n. \end{aligned} \tag{41}$$

Function $f_{\zeta i}(x,y)$ allows to calculate the angle of the vector (x,y); this angle lies into the set $[\zeta_i, 2\pi + \zeta_i)$. Parameter ζ_i defines the range of the function $f_{\zeta i}$. It also defines the range of mapping ϕ_1 as follows: let be $\mathbb{R}^{2n}$ the domain of ϕ_1, then:

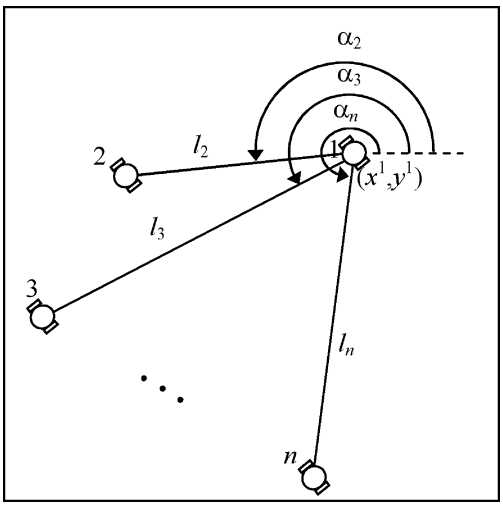


Fig. 2. First way to define the formation variables.

$$\begin{aligned} \Re(\phi_1) = \mathbb{R} \times \mathbb{R} \times \mathbb{R} \times [\varsigma_2, 2\pi + \varsigma_2) \times \cdots \times \mathbb{R} \\ \times [\varsigma_n, 2\pi + \varsigma_n), \end{aligned}$$

where $\Re(\phi_1)$ is the range of mapping ϕ_1. Angle α_{i} presents a discontinuity at ζ_{i}, which should be avoided during the evolution of the control system.

The inverse mapping $\xi = \phi_1^{-1}(z^1)$ is computed as follows:

$$\begin{aligned} x^1 &= x^1 \\ y^1 &= y^1 \\ x^i &= x^1 + l_i \cos\alpha_i; \quad i = 2, 3, \ldots, n \\ y^i &= y^1 + l_i \sin\alpha_i; \quad i = 2, 3, \ldots, n. \end{aligned} \tag{42}$$

The Jacobian matrix $\bar{J}(z^1)$ is:

$$\bar{J}(z^1) = \begin{bmatrix} I_{2\times2} & 0 & 0 & 0 & \cdots & 0 & 0 \\ I_{2\times2} & \bar{J}_{s2} & 0 & 0 & \cdots & 0 & 0 \\ I_{2\times2} & 0 & \bar{J}_{s3} & 0 & \cdots & 0 & 0 \\ \vdots & \vdots & \vdots & \vdots & \vdots & \vdots & \vdots \\ I_{2\times2} & 0 & 0 & 0 & \cdots & 0 & \bar{J}_{sn} \end{bmatrix}, \tag{43}$$

where $I_{2\times2}$ is a 2×2 identity matrix; and

$$\bar{J}_{si} = \begin{bmatrix} \cos\alpha_i & -l_i \sin\alpha_i \\ \sin\alpha_i & l_i \cos\alpha_i \end{bmatrix}; \quad i = 2, 3, \ldots, n. \tag{44}$$

Let:

$$K_j = \begin{bmatrix} K_{j1} & 0 & 0 & \cdots & 0 & 0 \\ 0 & K_{j2} & 0 & \cdots & 0 & 0 \\ \vdots & \vdots & \vdots & \vdots & \vdots & \vdots \\ 0 & 0 & 0 & \cdots & 0 & K_{jn} \end{bmatrix}; \quad j = 1, 2; \tag{45}$$

https://doi.org/10.1017/S0263574707004092 Published online by Cambridge University Press

$$z_1^1 = \begin{bmatrix} x^1 \\ y^1 \end{bmatrix}; \quad z_{1d}^1 = \begin{bmatrix} x_d^1 \\ y_d^1 \end{bmatrix};$$

$$z_i^1 = \begin{bmatrix} l_i \\ \alpha_i \end{bmatrix}; \quad z_{id}^1 = \begin{bmatrix} l_{id} \\ \alpha_{id} \end{bmatrix}; \quad i = 2, 3, \ldots, n; \tag{46}$$

$$\tilde{z}_i^1 = z_{id}^1 - z_i^1; \quad i = 1, 2, \ldots, n; \tag{47}$$

where K_{ji}>0 is a 2×2 matrix; x_d^1, y_d^1, l_{id}, α_{id} are the desired formation variables. Then, the formation control law can be expressed as follows:

$$\upsilon^1 = S_1, \tag{48}$$

$$\upsilon^i = S_1 + \bar{J}_{si} S_i + \dot{\bar{J}}_{si} \dot{z}_i^1; \quad i = 2, 3, \ldots, n, \tag{49}$$

where $S_i = K_{1i}\tilde{z}_i^1 + K_{2i}\dot{\tilde{z}}_i^1 + \ddot{z}_{id}^1$, $i = 1, 2, \ldots, n$. Now, it is easy to add more robots to the formation, because every new robot uses the formation control of (49). Every new robot only needs to sense the leader states and define its desired position with respect to robot 1.

The stability of the formation control (48) and (49) follows the general proof of Section 4, because this formation control is just the result from partitioning the formation control (31). In [9] the formation control is valid when considering one leader, or when a follower is defined as the leader of another follower. In the formation control (48) and (49), however, only one leader is used; if we want that a follower become the leader of another follower, we have to search for another partition of the formation control (31).

In this formation control, the control of robot 1 is not affected by the state of the other robots, as noted in (48). The control of the i-th robot is affected only by the state of robot 1.

Second mapping ϕ_1

Choosing the formation variables as in Fig. 3, the following mapping ϕ_1 is obtained:

$$z^1 = \phi_1(\xi) = [x_{cen} \quad y_{cen} \quad l_2 \quad \alpha_2 \quad l_3 \quad \alpha_3 \quad \cdots \quad l_n \quad \alpha_n]^T, \tag{50}$$

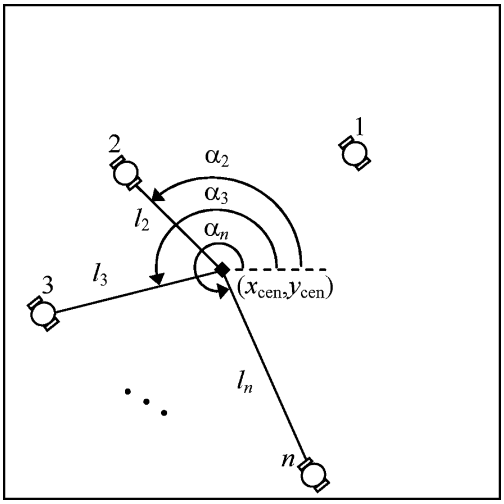


Fig. 3. Second way to define the formation variables.

where

$$x_{cen} = \frac{1}{n}\sum_{j=1}^{n} x^j; \quad y_{cen} = \frac{1}{n}\sum_{j=1}^{n} y^j,$$

$$l_i = \sqrt{(x^i - x_{cen})^2 + (y^i - y_{cen})^2}; \quad i = 2, 3, \ldots, n, \tag{51}$$

$$\alpha_i = f_{\zeta i}(x^i - x_{cen}, y^i - y_{cen}); \quad i = 2, 3, \ldots, n.$$

The inverse mapping $\xi = \phi_1^{-1}(z^1)$ is computed as follows:

$$x^1 = x_{cen} - \sum_{i=2}^{n} (l_i \cos\alpha_i),$$

$$y^1 = y_{cen} - \sum_{i=2}^{n} (l_i \sin\alpha_i), \tag{52}$$

$$x^i = x_{cen} + l_i \cos\alpha_i; \quad i = 2, 3, \ldots, n,$$

$$y^i = y_{cen} + l_i \sin\alpha_i; \quad i = 2, 3, \ldots, n.$$

The Jacobian matrix $\bar{J}(z^1)$ is

$$\bar{J}(z^1) = \begin{bmatrix} I_{2\times2} & -\bar{J}_{s2} & -\bar{J}_{s3} & -\bar{J}_{s4} & \cdots & -\bar{J}_{s(n-1)} & -\bar{J}_{sn} \\ I_{2\times2} & \bar{J}_{s2} & 0 & 0 & \cdots & 0 & 0 \\ I_{2\times2} & 0 & \bar{J}_{s3} & 0 & \cdots & 0 & 0 \\ \vdots & \vdots & \vdots & \vdots & \vdots & \vdots & \vdots \\ I_{2\times2} & 0 & 0 & 0 & \cdots & 0 & \bar{J}_{sn} \end{bmatrix}, \tag{53}$$

where $I_{2\times2}$ is a 2×2 identity matrix; and $\bar{J}_{si}$ is computed as in (44). Let us consider:

$$z_1^1 = \begin{bmatrix} x_{cen} \\ y_{cen} \end{bmatrix}; \quad z_{1d}^1 = \begin{bmatrix} x_{cend} \\ y_{cend} \end{bmatrix},$$

$$z_i^1 = \begin{bmatrix} l_i \\ \alpha_i \end{bmatrix}; \quad z_{id}^1 = \begin{bmatrix} l_{id} \\ \alpha_{id} \end{bmatrix}; \quad i = 2, 3, \ldots, n,$$

$$\tilde{z}_i^1 = z_{id}^1 - z_i^1; \quad i = 1, 2, \ldots, n,$$

where x_{cend}, y_{cend}, l_{id}, α_{id} are the desired formation variables. Then, the formation control law can be expressed as follows:

$$\upsilon^1 = S_1 - \sum_{i=2}^{n} \left(\bar{J}_{si} S_i + \dot{\bar{J}}_{si} \dot{z}_i^1\right), \tag{54}$$

$$\upsilon^i = S_1 + \bar{J}_{si} S_i + \dot{\bar{J}}_{si} \dot{z}_i^1; \quad i = 2, 3, \ldots, n, \tag{55}$$

where $S_i = K_{1i}\tilde{z}_i^1 + K_{2i}\dot{\tilde{z}}_i^1 + \ddot{z}_{id}^1$, $i = 1, 2, \ldots, n$; K_{ji} is obtained from (45). In this second formation control it is also easy to add more robots to the formation, because every new robot uses the formation control of (55). Every new robot needs to know the formation centroid's coordinates and to define its desired position with respect to this centroid. Besides, the formation controls of the earliest robots have to know the new centroid, and new terms have to be added to the summation in (54).

https://doi.org/10.1017/S0263574707004092 Published online by Cambridge University Press

The stability of the formation control (54) and (55) follows the general proof of Section 4, because this formation control is the result of just partitioning the formation control (31). In this formation control, the control of the i-th robot is affected by the states of the other robots.

6. Obstacle Avoidance

The formation obstacle avoidance strategy presented in this section is based on the concept of impedance with fictitious forces [17], [20], [8]. In [17], a fictitious force modifies the desired trajectory by means of an impedance function in order to avoid an obstacle. In the present work, this concept is used with an additional perpendicular fictitious force f_{I2}. Besides, the case of rigid formation obstacle avoidance is considered, that is the robots avoid the obstacle while maintaining its desired formation. The proposed strategy is based on a dynamical formation perimeter that will contain the formation and will interact with the obstacle. The aim is to avoid the perimeter collide with the obstacle. A simple formation perimeter is proposed, which allows the formation to avoid the obstacle while evolving with a short and efficient trajectory.

Let us consider the formation perimeter of Fig. 4. The way to construct this perimeter is by drawing two lines collinear to vector T_I that enclose all the robots. Vector T_I is in general the desired velocity of the formation. Then, two semicircles that connect the two lines are drawn as in Fig. 4. The lines and semicircles are drawn so as to achieve the shortest perimeter.

In Fig. 4, h_I is the obstacle position; p_m, p_{m2}, and r_m define the formation perimeter; d_I is the smallest vector connecting the formation perimeter with h_I; f_{I1}, and f_{I2} are fictitious forces collinear and perpendicular to d_I; β_I is the angle defined by vectors d_I and T_I; d_{max} defines a repulsive zone around the obstacle; d_{min} represents the minimum distance for non-contact of the formation perimeter with the obstacle. The vector T_I can be expressed as follows:

$$T_I = \begin{cases} \dot{c}_{md} & \text{if } \|\dot{c}_{md}\| \neq 0 \\ c_{md} - c_m & \text{if } \|\dot{c}_{md}\| = 0, \end{cases} \tag{56}$$

where c_m and c_{md} are the formation position and the desired formation position. In the previous equation, it is assumed that $c_{md} \neq c_m$, when $\|\dot{c}_{md}\| = 0$. Generally, if $c_{md} = c_m$ and $\|\dot{c}_{md}\| = 0$, the robot formation tends to stop and does not need an obstacle avoidance strategy. Let <O> be a relative frame system which origin is attached to the absolute coordinate origin and which x_o-axis is collinear to vector T_I.

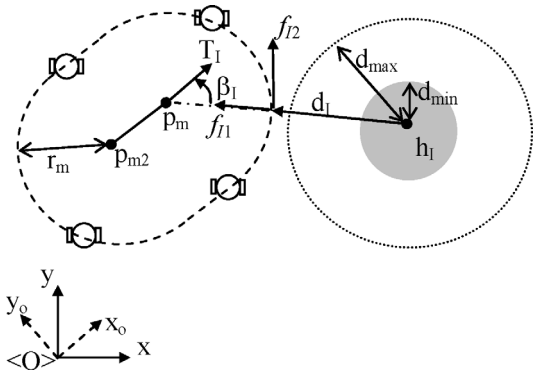


Fig. 4. Fictitious force that the obstacle exerts over the formation. The dashed curve shows the formation perimeter, and the dotted circle shows the repulsive zone.

Now, it is presented the way to compute the formation perimeter variables and the vector d_I. Let $h_o^i = [\,x_o^i \;\; y_o^i\,]^T$ and $h_{Io} = [\,x_{Io} \;\; y_{Io}\,]^T$ be the positions of the i-th robot and obstacle respectively, measured with respect to frame <O>. Then:

$$r_m = \left(\max_i \left(y_o^i\right) - \min_i \left(y_o^i\right)\right) \Big/ 2,$$

$$y_{mo} = \max_i \left(y_o^i\right) - r_m,$$

$$x_{mo} = \max_i \left(x_o^i - \sqrt{r_m^2 - \left(y_o^i - y_{mo}\right)^2}\right),$$

$$x_{m2o} = \min_i \left(x_o^i + \sqrt{r_m^2 - \left(y_o^i - y_{mo}\right)^2}\right),$$

$$p_{mo} = [\,x_{mo} \;\; y_{mo}\,]^T; \quad p_{m2o} = [\,x_{m2o} \quad y_{mo}\,]^T,$$

$$v_{pho} = \begin{cases} p_{mo} - h_{Io} & \text{if } x_{Io} > x_{mo} \\ [0(y_{mo} - y_{Io})]^{\mathrm{T}} & \text{if } x_{Io} \leq x_{mo} \text{ and } x_{Io} \geq x_{m2o}, \\ p_{m2o} - h_{Io} & \text{if } x_{Io} < x_{m2o} \end{cases}$$

$$d_{I\mu o} = v_{pho}/\|v_{pho}\|; \; \|d_I\| = \|v_{pho}\| - r_m, \tag{57}$$

where p_{mo}, p_{m2o} and $d_{I\mu o}$ are the vectors p_m, p_{m2} and $d_{I\mu}$ expressed in terms of frame <O>. The vector $d_{I\mu}$ is the unitary vector of d_I.

The fictitious force f_{I1} is computed as follows [8], [20]:

$$f_{I1} = \begin{cases} (a_I - b_I(\|d_I\| - d_{\min})^{n_I})d_{I\mu} & \text{if } \|d_I\| < d_{\max} \\ 0 & \text{if } \|d_I\| \geq d_{\max} \end{cases}, \tag{58}$$

where a_I, b_I, n_I, are positive constants such that $a_I - b_I\,(d_{\max} - d_{\min})^{n_I} = 0$. Constant n_I defines how reactive is the interaction at the repulsion zone of the obstacle.

The fictitious force f_{I2} allows the formation to go easily around the obstacle when $\beta_I \approx 0$. The fictitious force f_{I2} is computed as follows:

$$f_{I2} = -\rho_I sign(\beta_I) e^{-\beta_I^2} R\,(\pi/2)\, d_{I\mu}\, \|f_{I1}\|; \quad \rho_I > 0, \tag{59}$$

where ρ_I is a weight for f_{I2}; $R\,(\pi/2)$ is the matrix that rotates a vector $\pi/2$ radians. The fictitious force f_{I2} will increase as β_I decreases, thus giving an effective deviation force from the obstacle.

Now, a motion-based impedance control is used (see Fig. 5) [19]; here, the reference formation motion is deviated by a deviation signal from the impedance block. In Fig. 5, $p = d/dt$; I_I, D_I, K_I are the so-called inertia, damping, and elasticity matrices. f_I is computed as follows:

https://doi.org/10.1017/S0263574707004092 Published online by Cambridge University Press

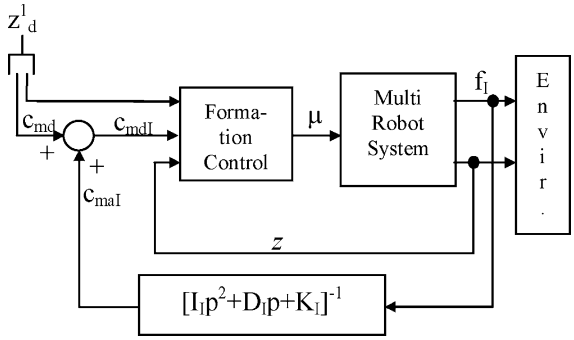


Fig. 5. Formation motion-based impedance control.

$$f_I = f_{I1} + f_{I2}.$$

In the formation control, the desired formation position, as well as the desired velocity and desired acceleration are replaced by c_{mdI}, $\dot{c}_{mdI}$, $\ddot{c}_{mdI}$, where $c_{mdI} = c_{md} + c_{maI}$.

When approaching an obstacle, a fictitious force f_I generates the deviation signal c_{maI} through the inverse impedance as shown in Fig. 5. Therefore, the desired formation trajectory c_{mdI} is deviated smoothly and the formation avoids the obstacle.

These matrices in the impedance function of the outer loop in Fig. 5, define the interaction dynamics between the formation and the obstacle. Stability of the whole system is preserved for I_I, D_I, K_I real positive definite symmetric matrices.

7. Experiments

Experiments to test the control of robot formations were performed using three Pioneer mobile robots, one of which equipped with an omnidirectional camera system mounted on it (see Fig. 6) and an on-board computer for image processing. An off-board computer is used to monitor and control the robots through wireless Ethernet and a radio modem.

The identification of the robot model was performed by using least squares estimation [2] applied to a filtered regression model [18] obtained from (10). The identified parameters of the robot with the omnidirectional camera system and on-board computer are (robot #1):

$$\bar{\theta}_1^0 = 0.26038, \quad \bar{\theta}_2^0 = 0.25095, \quad \bar{\theta}_3^0 = -0.00049969,$$
$$\bar{\theta}_4^0 = 0.99646, \quad \bar{\theta}_5^0 = 0.002629, \quad \bar{\theta}_6^0 = 1.0768;$$

the identified parameters of the robot #2 (with on-board computer) are:

$$\bar{\theta}_1^0 = 0.3037, \quad \bar{\theta}_2^0 = 0.2768, \quad \bar{\theta}_3^0 = -0.0004018,$$
$$\bar{\theta}_4^0 = 0.983516, \quad \bar{\theta}_5^0 = 0.003818, \quad \bar{\theta}_6^0 = 1.07253;$$

and the identified parameters of the robot #3 (without on-board computer) are:

$$\bar{\theta}_1^0 = 0.1932, \quad \bar{\theta}_2^0 = 0.137672, \quad \bar{\theta}_3^0 = 0.0003524,$$
$$\bar{\theta}_4^0 = 0.98331, \quad \bar{\theta}_5^0 = -0.0104165, \quad \bar{\theta}_6^0 = 0.983714.$$

In (16), $C_{h\delta} = 0.3$ m/s and $\omega_{max} = 1.745$ rad/s are considered, thus $|a| \geq 0.172$ m. Then, a constant $a = 0.2$ m was chosen.

The first mapping presented in Section 5 is chosen for the experiments. The following control parameters are used in the experiments:

$$K_1 = diag(0.2, 0.2, 0.4, 0.4, \ 0.8, 0.8),$$
$$K_2 = diag(2\sqrt{0.2}, 2\sqrt{0.2}, 2\sqrt{0.4}, 2\sqrt{0.4}, 2\sqrt{0.8}, 2\sqrt{0.8}), \tag{60}$$

where *diag(.)* represents a diagonal matrix. The initial velocities of the robots are zero.

In a first experiment, it is performed a triangle formation control following a curve trajectory. The robots move an object as can be seen in Fig. 6; one robot pushes the object and the other robots confine it on both sides. The desired formation variables are chosen as:

$$z_d^1 = \begin{bmatrix} x_d^1 \\ y_d^1 \\ l_{2d} \\ \alpha_{2d} \\ l_{3d} \\ \alpha_{3d} \end{bmatrix} = \begin{bmatrix} 0.45 + 2.5\sin(0.03t) \\ 2.5 - 2.5\cos(0.03t) \\ 0.9 \\ -0.4 + 0.03t \\ 0.9 \\ 0.4 + 0.03t \end{bmatrix}; \tag{61}$$

$$\dot{z}_d^1 = \begin{bmatrix} 0.075\cos(0.03t) \\ 0.075\sin(0.03t) \\ 0 \\ 0.03 \\ 0 \\ 0.03 \end{bmatrix}; \quad \ddot{z}_d^1 = \begin{bmatrix} -0.00225\sin(0.03t) \\ 0.00225\cos(0.03t) \\ 0 \\ 0 \\ 0 \\ 0 \end{bmatrix}. \tag{62}$$

In z_d^1, the positions and distances are expressed in meters and the angles are expressed in radians. Figures 7 and 8 present the experimental results of the formation control, showing a good tracking performance of the desired formation. After 12.5 seconds of evolution, the formation errors are smaller than 0.05 m (distance errors) and smaller than 0.03 rad (angle error). These results validate the controller design presented in previous sections.



Fig. 6. Mobile robots and omnidirectional camera.

https://doi.org/10.1017/S0263574707004092 Published online by Cambridge University Press

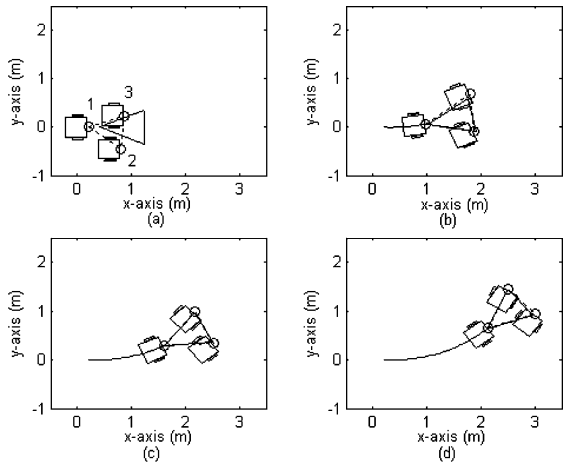


Fig. 7. Formation trajectory, the solid line triangle represents the desired formation.

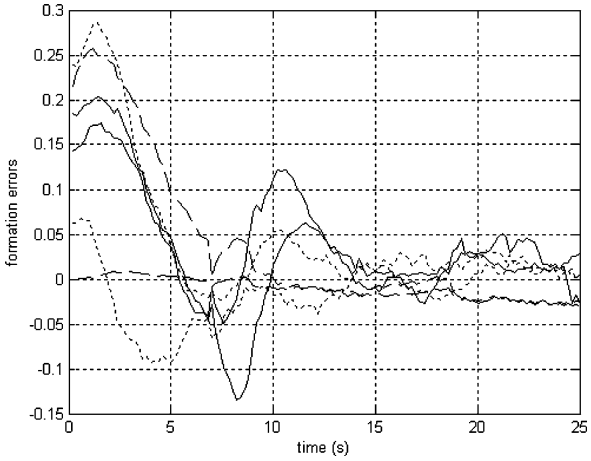


Fig. 8. Formation error through time; the dashed lines are position errors (m), the solid lines are distance errors (m) and the dotted lines are angle errors (rad).

In a second experiment, a triangle formation control avoiding an obstacle is made. The desired formation variables are chosen as:

$$z_d^1 = \begin{bmatrix} x_d^1 \\ y_d^1 \\ l_{2d} \\ \alpha_{2d} \\ l_{3d} \\ \alpha_{3d} \end{bmatrix} = \begin{bmatrix} 0.2 + 0.075t \\ 0 \\ 0.7 \\ \pi + 0.4 \\ 0.6 \\ -\pi/2 \end{bmatrix};$$

$$\dot{z}_d^1 = \begin{bmatrix} 0.075 \\ 0 \\ 0 \\ 0 \\ 0 \\ 0 \end{bmatrix}; \quad \ddot{z}_d^1 = \begin{bmatrix} 0 \\ 0 \\ 0 \\ 0 \\ 0 \\ 0 \end{bmatrix}. \tag{63}$$

Again, in z_d^1, the positions and distances are expressed in meters and the angles are given in radians. The parameters of the obstacle avoidance strategy are selected as:

$$d_{min} = 0.375; d_{max} = 0.775; a_I = 1.3; n_I = 1; \rho_I = 0.75,$$

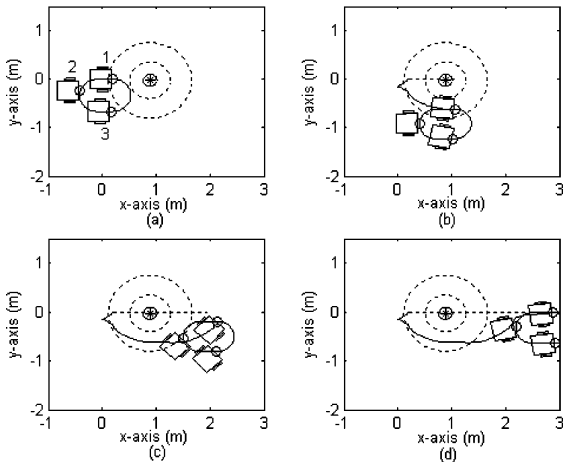


Fig. 9. Formation trajectory while avoiding an obstacle. The dotted line represents the desired trajectory while the solid line is the actual trajectory. The dotted circles define the repulsive zone and the minimum distance for non-contact.

$$I_I = \begin{bmatrix} 1 & 0 \\ 0 & 1 \end{bmatrix}; \quad D_I = \begin{bmatrix} 4 & 0 \\ 0 & 4 \end{bmatrix}; \quad K_I = \begin{bmatrix} 1 & 0 \\ 0 & 1 \end{bmatrix}.$$

Figure 9 presents the experimental results of the formation control while avoiding an obstacle. It is shown a good performance of the obstacle avoidance strategy while maintaining a rigid formation during the maneuvering.

8. Conclusion

A complete dynamic model of a unicycle-like mobile robot and its linear parameterization were presented. An input-output feedback linearization of the model was performed. Then, after defining a formation state vector, a formation control of the multi-robot system was designed using inverse dynamics. The controller allows the tracking of desirable formations evolving on the plane. The use of the formation states, both in the model and in the formation control design of the multi-robot system, allows achieving a better design of the time evolution of the formation. A decentralized formation control and a centralized formation control, both scalable to any number of robots, were presented. Good rigid formation obstacle avoidance was obtained.

Future work will delve into issues concerning uncertainties or changes in model parameters, by resorting to adaptive and robust control strategies to guarantee good control performance. Also, hybrid strategies applied to formation control could help to enhance formation control performance in some robotic tasks.

Appendix

Dynamic robot model

Combining the second and third equations of (1) we obtain,

$$\dot{\omega} = \frac{d}{2I_z}(F_{rrx'} - F_{rlx'}) + \frac{e}{I_z}F_{ey'} + \frac{c}{I_z}F_{cy'} + \frac{1}{I_z}\tau_e - \frac{mb}{I_z}(\dot{\tilde{u}} + u\omega). \tag{64}$$

https://doi.org/10.1017/S0263574707004092 Published online by Cambridge University Press

Substituting (4) into (5) and re-arranging,

$$F_{rrx'} = \frac{k_a}{R_a R_t}(v_r - k_b\omega_r) - \frac{I_e}{R_t}\dot{\omega}_r - \frac{B_e}{R_t}\omega_r,$$
$$F_{rlx'} = \frac{k_a}{R_a R_t}(v_l - k_b\omega_l) - \frac{I_e}{R_t}\dot{\omega}_l - \frac{B_e}{R_t}\omega_l. \tag{65}$$

Now, re-arranging the first and the second expressions of (4),

$$\omega_r + \omega_l = \frac{2}{r}u - \frac{1}{r}\left(u_r^s + u_l^s\right),$$
$$\omega_r - \omega_l = \frac{d}{r}\omega - \frac{1}{r}\left(u_r^s - u_l^s\right), \tag{66}$$

Combining the equations (66) and (6), we obtain,

$$\begin{aligned} v_r + v_l &= 2k_{PT}\left(u_{ref} - u + \frac{1}{2}\left(u_r^s + u_l^s\right)\right) \\ &\quad - 2k_{DT}\left(\dot{u} - \frac{1}{2}\left(\dot{u}_r^s + \dot{u}_l^s\right)\right), \\ v_r - v_l &= 2k_{PR}\left(\omega_{ref} - \omega + \frac{1}{d}\left(u_r^s - u_l^s\right)\right) \\ &\quad - 2k_{DR}\left(\dot{\omega} - \frac{1}{d}\left(\dot{u}_r^s - \dot{u}_l^s\right)\right). \end{aligned} \tag{67}$$

Substituting the second in the third equation of (4),

$$\bar{u} = b\omega + \bar{u}^s. \tag{68}$$

Also, by substituting (65) into (64), and then using the second expression of (66), the second expression of (67) and (68) in the resulting equation, we obtain,

$$\begin{aligned} \bar{\theta}_2^0\dot{\omega} &= \omega_{ref} - \bar{\theta}_6^0\omega + \frac{1}{d}\bar{\theta}_6^0\left(u_r^s - u_l^s\right) \\ &\quad + \left(\frac{k_{DR}}{dk_{PR}} + \frac{R_a I_e}{2k_{PR}k_a r}\right)\left(\dot{u}_r^s - \dot{u}_l^s\right) \\ &\quad + \frac{R_a R_t}{dk_{PR}k_a}(eF_{ey'} + cF_{cy'} + \tau_e) - \bar{\theta}_5^0\dot{\bar{u}}^s - \bar{\theta}_5^0 u\omega. \end{aligned} \tag{69}$$

Now, substituting (65) into the first equation of (1), and then using the first equation of (66), the first equation of (67) and (68) in the resulting equation, we obtain,

$$\begin{aligned} \bar{\theta}_1^0\dot{u} &= u_{ref} - \bar{\theta}_4^0 u + \frac{1}{2}\bar{\theta}_4^0\left(u_r^s + u_l^s\right) \\ &\quad + \left(\frac{k_{DT}}{2k_{PT}} + \frac{I_e R_a}{2k_{PT}k_a r}\right)\left(\dot{u}_r^s + \dot{u}_l^s\right) \\ &\quad + \frac{R_a R_t}{2k_{PT}k_a}\left(F_{ex'} + F_{cx'}\right) + \bar{\theta}_3^0\omega^2 + \frac{R_a R_t m}{2k_{PT}k_a}\omega\bar{u}^s. \end{aligned} \tag{70}$$

Finally, substituting (68) into (2), then using this result as well as equations (69) and (70), the dynamic robot model (7) is thus obtained.

References

1. G. Antonelli and S. Chiaverini, "Kinematic Control of a Platoon of Autonomous Vehicles," *IEEE International Conference on Robotics and Automation*, Taipei, Taiwan (September 2003) pp. 1464–1469.
2. K. J. Aström and B. Wittenmark, *Adaptive Control* (Addison-Wesley, 1995).
3. T. Balch and R. C. Arkin, "Behavior-Based Formation Control for Multirobot teams," *IEEE Transactions on Robotics and Automation*, 14(6) (December 1998) pp. 926–939.
4. T. Balch and M. Hybinette, "Social Potentials for Scalable Multi-Robot Formations," *IEEE International Conference on Robotics and Automation*, San Francisco (April 2000) pp. 73–80.
5. C. Belta and V. Kumar, "Trajectory Design for Formations of Robots by Kinetic Energy Shaping," *IEEE International Conference on Robotics and Automation*, Washington, DC (May 2002) pp. 2593–2598.
6. B. E. Bishop, "Dynamics-Based Control of Robotic Swarms," *IEEE International Conference on Robotics and Automation*, Orlando, Florida (May 2006) pp. 2763–768.
7. F. D. Boyden and S. A. Velinsky, "Dynamic Modeling of Wheeled Mobile Robots for High Load Applications," *IEEE International Conference on Robotics and Automation*, **4**, (1994), pp. 3071–3078.
8. R. Carelli, O. Nasisi F. Roberti and S. Tosetti, "Direct visual tracking control of remote cellular robots," *13th. Int. Symposium on Measurement and Control in Robotics – Towards advanced robots: Design, sensors, control, Applications* – ISMCR'03, Madrid (December 2003), pp. 11–12.
9. A. K. Das, R. Fierro, V. Kumar, J. P. Ostrowski, J. Spletzer and C. J. Taylor, "A vision-Based Formation Control Framework," *IEEE Transactions on Robotics and Automation*, **18**(5), (October 2002) pp. 813–825.
10. J. P. Desai, J. Ostrowski and V. Kumar, "Controlling Formations of Multiple Mobile robots," In *Proc. IEEE International Conference Robotics and Automation*, Leuven, Belgium (May 1998) pp. 2864–2869.
11. R. Fierro, A. K. Das, V. Kumar, and J. P. Ostrowski, "Hibrid Control of Formations of Robots," *In Proc. IEEE International Conference Robotics and Automation*, Seoul, Korea (May 2001) pp. 3672–3677.
12. J. Fredslund and M. J. Mataric, "Robot Formations Using only Local Sensing and Control," *IEEE International Symposium on Computational Intelligence in Robotics and Automation*, Banff, Alberta, Canada (July 2001) pp. 308–313.
13. R. Kelly, R. Carelli, J. M. Ibarra Zannatha and C. Monroy, "Formation Tracking Control of a Group of Mobile Robots," In Spanish. *VI Congreso Mexicano de Robótica*, COMRob, Torreón, Coahuila, Mexico (October 2004).
14. J. R. T. Lawton, R. W. Beard and B. J. Young, "A decentralized Approach to Formation Maneuvers," *IEEE Transactions on Robotics and Automation*, 19(6), (December 2003) pp. 933–941.
15. G. L. Mariottini, F. Morbidi, D. Prattichizzo, G. J. Pappas and K. Daniilidis, "Leader-Follower Formations: Uncalibrated Vision-Based Localization and Control," *IEEE International Conference on Robotics and Automation*, Roma (April 2007) pp. 2403–2408.
16. S. Monteiro, M. Vaz, and E. Bicho, "Attractor Dynamics Generates Robot Formations: From Theory to Implementation," *IEEE International Conference on Robotics and Automation*, New Orleans, LA (April 2004) pp. 2582–2587.
17. V. Mut, O. Nasisi, R. Carelli, and B. Kuchen, "Tracking Adaptive Impedance Robot Control with Visual Feedback", *IEEE International Conference on Robotics and Automation*, Leuven, Belgium (May 1998) pp. 2002–2007.
18. F. Reyes and R. Kelly, "On Parameter Identification of Robot Manipulator," *IEEE International Conference on Robotics and Automation*, Albuquerque, New Mexico (April 1997) pp. 1910–1915.

https://doi.org/10.1017/S0263574707004092 Published online by Cambridge University Press

19. L. Sciavicco and B. Siciliano, *Modelling and Control of Robot Manipulators* (Springer, 2000).
20. H. Secchi, R. Carelli, and V. Mut, "An Experience on Stable Control of Mobile Robots", *Latin American Applied Research*, Buenos Aires, Argentina, 33(4), (October 2003) pp. 379–386.
21. J. -J. Slotine and W. Li, *Applied Nonlinear Control* (Prentice Hall Int., 1991).
22. D. J. Stilwell and B. E. Bishop, "A Strategy for Controlling Autonomous Robot Platoons", *IEEE Conference on Decision and Control*, Sydney, Australia (December 2000) pp. 3483–3488.
23. K. H. Tan and M. A. Lewis, "Virtual structures for high-precision cooperative mobile robotic control," *International Conference on Intelligent Robots and Systems* 1 (November 1996) pp. 132–139.
24. M. Vidyasagar, *Nonlinear Systems Analysis* (Prentice-Hall Int., New Jersey, 1993).
25. H. Yamaguchi, T. Arai and G. Beni, "A distributed control scheme for multiple robotic vehicles to make group formations," *Robot. Auton. Sys.* 36, 125–147 (2001).
26. Y. Zhang, D. Hong, J. H. Chung and S. A. Velinsky, "Dynamic Model Based Robust Tracking Control of a Differentially Steered Wheeled Mobile Robot," *Proceedings of the American Control Conference*, Philadelphia, Pennsylvania (June 1998) pp. 850–855.

https://doi.org/10.1017/S0263574707004092 Published online by Cambridge University Press